Physical properties of noncentrosymmetric superconductor $LaIrSi_3$: A μSR study

V. K. Anand,[1,2,*] D. Britz,[3] A. Bhattacharyya,[1,3] D. T. Adroja,[1,3,†] A. D. Hillier,[1] A. M. Strydom,[3] W. Kockelmann,[1] B. D. Rainford,[4] and K. A. McEwen[5]

[1]*ISIS Facility, Rutherford Appleton Laboratory, Chilton, Didcot, Oxon OX11 0QX, United Kingdom*

[2]*Helmholtz-Zentrum Berlin für Materialien und Energie, Hahn-Meitner Platz 1, D-14109 Berlin, Germany*

[3]*Highly Correlated Matter Research Group, Physics Department, University of Johannesburg, P. O. Box 524, Auckland Park 2006, South Africa*

[4]*Physics Department, University of Southampton, Southampton SO17 1BJ, United Kingdom*

[5]*Department of Physics and Astronomy and London Centre for Nanotechnology, University College London, Gower Street, London WC1E 6BT, United Kingdom*

(Received 21 May 2014; revised manuscript received 8 July 2014; published 23 July 2014)

The results of heat capacity $C_p(T,H)$ and electrical resistivity $\rho(T,H)$ measurements down to 0.35 K as well as muon spin relaxation and rotation (μSR) measurements on the noncentrosymmetric superconductor $LaIrSi_3$ are presented. Powder neutron diffraction confirmed the reported noncentrosymmetric body-centered tetragonal $BaNiSn_3$-type structure (space group $I4mm$) of $LaIrSi_3$. The bulk superconductivity is observed below $T_c = 0.72(1)$ K. The intrinsic $\Delta C_e/\gamma_n T_c = 1.09(3)$ is significantly smaller than the BCS value of 1.43, and this reduction is accounted for by the α model of BCS superconductivity. The analysis of the superconducting-state $C_e(T)$ data by the single-band α model indicates a moderately anisotropic order parameter with the s-wave gap $\Delta(0)/k_B T_c = 1.54(2)$, which is lower than the BCS value of 1.764. Our estimates of various normal- and superconducting-state parameters indicate a weakly coupled electron-phonon-driven type-I s-wave superconductivity in $LaIrSi_3$. The μSR results also confirm the conventional type-I superconductivity in $LaIrSi_3$ with a preserved time-reversal symmetry and hence a singlet pairing superconducting ground state.

DOI: 10.1103/PhysRevB.90.014513 PACS number(s): 74.70.Dd, 74.25.Bt, 76.75.+i

I. INTRODUCTION

The noncentrosymmetric superconductors (NCSs) that allow mixing between spin-singlet and spin-triplet parity and exhibit exotic superconducting properties through the antisymmetric spin-orbit coupling (ASOC) are of great interest in current research activities on superconductivity [1]. The NCSs lack inversion symmetry in their crystal structure, which leads to a nonuniform lattice potential and hence introduces an antisymmetric spin-orbit coupling. The ASOC removes the spin degeneracy of conduction-band electrons; that is, the spin-up and spin-down energy bands split, and the two electrons forming a Cooper pair no longer belong to the *same* Fermi surface as in the conventional superconductors. An important consequence of Cooper pair formation by the electrons belonging to two *different* Fermi surfaces of spin-up and spin-down bands is that the Cooper pair wave function of NCSs can no longer be classified by its parity as a pure spin-singlet or spin-triplet pairing, instead results in a parity mixing of spin singlet-triplet states [2–6]. For centrosymmetric superconductors to which most of the known superconductors belong the spin-up and spin-down energy bands of the conduction electrons are degenerate when time-reversal symmetry is conserved. The structural inversion symmetry thus has a key role in determining the superconducting properties, and a number of unusual phenomena can be observed in such noncentrosymmetric materials [2–6].

First such unusual superconducting behavior was observed in the heavy-fermion superconductor $CePt_3Si$, which crystallizes in a tetragonal structure (space group $P4mm$) that lacks mirror symmetry along the c axis and undergoes an antiferromagnetic transition below $T_N = 2.2$ K and becomes superconducting at the critical temperature $T_c = 0.75$ K that coexists with antiferromagnetic ordering [7]. The upper critical field $H_{c2} \approx 5$ T is very high compared to the Pauli paramagnetic limiting field of $\sim$1 T, indicating a spin-triplet pairing [7]. For a spin-singlet paring, Pauli paramagnetic limiting is expected. On the other hand, for a system without inversion symmetry spin-triplet pairing is not permitted [1]. These contradicting situations are accounted for by mixed spin singlet-triplet states of the order parameter [6]. The irreducible representation point group for the tetragonal structure of $CePt_3Si$ is C_{4v}, in which Rashba-type ASOC exists, which provides the key to understanding the intriguing superconducting behavior of $CePt_3Si$ [7–9]. Following $CePt_3Si$ many NCSs have been identified that present interesting superconducting properties, including $Li_2(Pd,Pt)_3B$ [10,11], $CeRhSi_3$ [12,13], $CeIrSi_3$ [14], $CeCoGe_3$ [15,16], $CeIrGe_3$ [17], $LaNiC_2$ [18–20], $BaPtSi_3$ [21], $(Rh,Ir)Ga_9$ [22,23], $Mg_{10}Ir_{19}B_{16}$ [24], Mo_3Al_2C [25], $LaRhSi_3$ [26], $Ca(Ir,Pt)Si_3$ [27], Re_3W [28], $Nb_{0.18}Re_{0.12}$ [29], Re_6Zr [30], $La(Pd,Pt)Si_3$ [31], $Ca_3Ir_4Ge_4$ [32], etc.

The Ce-based NCSs $CeRhSi_3$, $CeIrSi_3$, $CeCoGe_3$, and $CeIrGe_3$ crystallize with $BaNiSn_3$-type tetragonal structure (space group $I4mm$), which lacks mirror plane symmetry along the c axis and belongs to the same point group, C_{4v}, as $CePt_3Si$. Thus, like $CePt_3Si$, a Rashba-type ASOC is present in these $CeMX_3$ compounds too, leading to an exotic superconducting ground state in them [12–17,33–35]. Like $CePt_3Si$, they also exhibit heavy-fermion behavior and undergo a long-range antiferromagnetic ordering; however, they

*vivekkranand@gmail.com
†devashibhai.adroja@stfc.ac.uk

become superconducting only under the application of pressure [12–17,33–35]. The above-mentioned Ce-based NCSs are situated close to a magnetic quantum critical point, making it difficult to explore the effects of ASOC and inversion symmetry breaking on superconductivity. Therefore nonmagnetic Rashba-type NCSs are essential for understanding the effect and extent of ASOC on the superconducting properties of these Ce-based NCSs. The reported nonmagnetic AMX_3 NCSs with $BaNiSn_3$-type tetragonal structure include $BaPtSi_3$ (T_c = 2.25 K), $LaRhSi_3$ [$T_c = 2.16(8)$ K], $CaIrSi_3$ ($T_c = 3.6$ K), $CaPtSi_3$ ($T_c = 2.3$ K), $LaPdSi_3$ [$T_c = 2.65(5)$ K], and $LaPtSi_3$ [$T_c = 1.52(6)$ K] [21,26,27,31]. All these nonmagnetic NCSs behave like a conventional *s*-wave superconductor without any noticeable effect from the absence of inversion symmetry in their crystal structure. Nevertheless, being isostructural, they provide a direct comparison with $CeMX_3$ NCSs and the investigations of these nonmagnetic NCSs connote the role of 4*f* moments in Ce NCSs. One important difference between the $CeMX_3$ NCSs and these nonmagnetic NCSs is that $CeMX_3$ exhibit superconductivity only at high pressures, whereas these nonmagnetic NCSs superconduct at ambient pressure. This difference may have its origin in magnetic pairing in Ce NCSs in contrast to phonon-mediated superconductivity in these nonmagnetic NCSs.

Theoretically, the Rashba-type ASOC has been studied extensively and is favored for investigations of NCSs; therefore compounds with tetragonal $BaNiSn_3$-type structure represent an important class of noncentrosymmetric materials. Continuing our work on $BaNiSn_3$-type structured materials, we have performed a comprehensive study of superconducting- and normal-state properties of NCS $LaIrSi_3$ using heat capacity C_p and electrical resistivity ρ versus temperature T measurements down to 0.35 K and muon spin relaxation and rotation (μSR) measurements down to 50 mK. The reported noncentrosymmetric body-centered tetragonal $BaNiSn_3$-type structure of $LaIrSi_3$ is confirmed by our room-temperature powder x-ray diffraction (XRD) and neutron diffraction. Superconductivity in $LaIrSi_3$ was reported about 30 years ago with T_c between 1.9 and 2.7 K based on resistivity measurement [36,37]. In a recent study Okuda *et al.* reported a superconducting transition at $T_c = 0.77$ K from the heat-capacity measurement on $LaIrSi_3$ [33]. Okuda *et al.* also carried out a de Haas–van Alphen (dHvA) effect study and found that as a result of Rashba-type ASOC the Fermi surface of $LaIrSi_3$ splits into two Fermi surfaces (spin-up and spin-down energy bands), which are separated by about 1000 K [33]. In our recent investigations of superconducting properties of NCS $LaRhSi_3$ we found a conventional type-I superconductivity with preserved time-reversal symmetry, however, with an unusual exponential evolution of the Sommerfeld coefficient γ with magnetic field which could be due to the reinforcement of ASOC with magnetic field [26]. Therefore in view of the unusual behavior of $LaRhSi_3$ and the strong effect of ASOC in $LaIrSi_3$ revealed by the dHvA effect study, it was felt necessary to investigate the superconducting properties of $LaIrSi_3$ in detail, which we present in this paper.

Our $C_p(T)$ data confirm bulk superconductivity in $LaIrSi_3$ below $T_c = 0.72(1)$ K, in agreement with the report by Okuda *et al.* [33]. However, $\rho(T)$ exhibits superconductivity at a higher $T_c = 1.45$ K, apparently due to filamentary nonbulk superconductivity. The normal-state ρ is metallic and well described by the Bloch-Grüneisen model of resistivity for $T \geqslant 1.6$ K. The low-T normal-state $C_p(T)$ gives an electronic coefficient $\gamma_n = 4.60(2)$ mJ/mol K^2 and a density of states at Fermi energy $\mathcal{D}(E_F) = 1.95(1)$ states/eV f.u. for both spin directions, where f.u. stands for formula unit. A sharp jump is observed at $T_c = 0.72(1)$ K in electronic heat capacity $C_e(T)$, with $\Delta C_e/\gamma_n T_c = 1.09(3)$, which is smaller than the BCS expected value of 1.43. Within the single-band picture the reduced value of $\Delta C_e/\gamma_n T_c$ can be attributed to an anisotropic energy gap in $LaIrSi_3$. We have analyzed the superconducting-state electronic heat-capacity data using the α model of BCS superconductivity [38–40], which suggests that the *s*-wave order parameter of $LaIrSi_3$ is anisotropic in momentum space, with an energy gap $\Delta(0)/k_B T_c = 1.54(2)$. We have estimated various normal- and superconducting-state parameters that indicate a weak-coupling type-I BCS superconductivity in the dirty limit. Our μSR investigations also confirm type-I superconductivity in $LaIrSi_3$. Further, μSR results also show that the time-reversal symmetry is preserved as is expected for a conventional *s*-wave singlet pairing superconductivity. No evidence of parity mixing is observed as one would have expected in view of splitting of spin-up and spin-down energy bands revealed by dHvA study [33].

II. EXPERIMENTAL DETAILS

A polycrystalline sample of $LaIrSi_3$ was prepared by the standard arc melting of a stoichiometric mixture of high-purity elements (La: 99.9%, Ir: 99.99%, Si: 99.999%) on a water-cooled copper hearth under the titanium-gettered inert argon atmosphere with several flips to ensure homogeneity. The arc-melted sample was further heat treated at 900 °C for a week under the dynamic vacuum. The crystal structure was determined by the powder XRD using Cu K_α radiation. The heat-capacity measurements were performed by the relaxation method with a physical properties measurement system (PPMS, Quantum Design, Inc.). The electrical resistivity measurements were performed by the standard four-probe ac technique using the PPMS. Temperatures down to 0.35 K were attained using a ^{3}He attachment to the PPMS.

Powder neutron diffraction (ND) measurement was performed at room temperature using the ROTAX diffractometer at the ISIS facility of the Rutherford Appleton Laboratory, Didcot, United Kingdom. The μSR measurements were carried out using the MuSR spectrometer at the ISIS facility with the detectors in both longitudinal and transverse configurations. A high-purity-silver plate was used to mount the sample, which gives only a nonrelaxing muon signal. The powdered sample was mounted on silver plate using diluted GE varnish that was covered with Kapton film. Temperatures down to 50 mK were achieved by cooling the sample in a dilution refrigerator. Correction coils were used to counter the effect of the stray fields at the sample position to within 1 μT.

III. CRYSTALLOGRAPHY

The room-temperature powder XRD data were analyzed by structural Rietveld refinement using the program FULLPROF [41]. The refinement confirmed the reported $BaNiSn_3$-

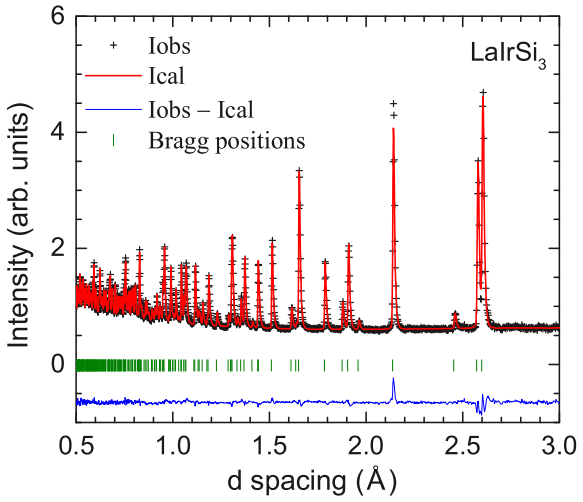

FIG. 1. (Color online) Powder neutron diffraction pattern of $LaIrSi_3$ recorded at room temperature. The solid line through the experimental points is the Rietveld refinement profile calculated for the noncentrosymmetric body-centered tetragonal $BaNiSn_3$-type structure (space group $I4mm$). The short vertical bars indicate the Bragg peak positions. The lowermost curve represents the difference between the experimental and calculated intensities.

type tetragonal structure (space group $I4mm$) of $LaIrSi_3$ and revealed the single-phase nature of the sample without any trace of the impurity phase. The single-phase nature of the whole bulk of the sample is further inferred from the Rietveld refinement of room-temperature powder neutron diffraction data that was performed using the program GSAS [42]. The neutron diffraction pattern and refinement profile for the noncentrosymmetric body-centered tetragonal $BaNiSn_3$-type structure are shown in Fig. 1. While refining, no improvement in the fit quality was observed upon refining the occupancies of atomic positions, and within the error bars the atomic occupancies were found to be unity; therefore in the final refinement we fixed the occupancies to unity. The crystallographic parameters

TABLE I. Crystallographic parameters obtained from the structural Rietveld refinement of room-temperature powder neutron diffraction data of $LaIrSi_3$. Profile reliability factor $R_p = 2.60\%$, and weighted profile R factor $R_{wp} = 2.33\%$.

Structure	$BaNiSn_3$-type tetragonal
Space group	$I4mm$ (No. 107)
Lattice parameters	
a (Å)	4.2784(3)
c (Å)	9.8308(7)
V_{cell} (Å^3)	179.95(4)

Atomic coordinates

Atom	Wyckoff position	x	y	z	U_{iso} (Å^2)
La	2a	0	0	0	0.0008(3)
Ir	2a	0	0	0.6554(2)	0.0021(3)
Si1	2a	0	0	0.4140(3)	0.0003(3)
Si2	4b	0	1/2	0.2624(2)	0.0033(3)

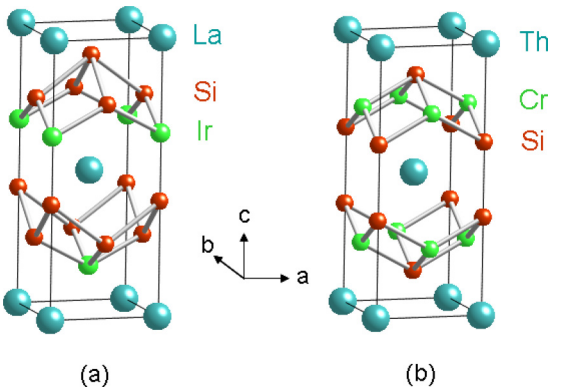

FIG. 2. (Color online) Comparison of (a) the $BaNiSn_3$-type noncentrosymmetric body-centered tetragonal structure ($I4mm$) of $LaIrSi_3$ and (b) the $ThCr_2Si_2$-type body-centered tetragonal crystal structure ($I4/mmm$).

obtained from the refinement of powder neutron diffraction are listed in Table I. Both ND and XRD data gave similar crystallographic parameters and agree well with the literature values [36,43].

The $BaNiSn_3$-type body-centered tetragonal structure (space group $I4mm$) of $LaIrSi_3$ is illustrated in Fig. 2 and is compared with the common $ThCr_2Si_2$-type body-centered tetragonal structure (space group $I4/mmm$). Like the $ThCr_2Si_2$-type structure, the $BaNiSn_3$-type structure is also a layered structure and a ternary derivative of $BaAl_4$-type structure [44]. The R (La, Th) atoms occupy identical positions in both structures and form a body-centered tetragonal sublattice. However, they differ in the positions of T (Ir, Cr) and Si atoms. The T atoms form a square sublattice in the ab plane in both structures, but they are rotated by 45° in the ab plane with respect to each other. Further, in the $ThCr_2Si_2$-type structure all the Si atoms occupy a single crystallographic site, whereas in the $BaNiSn_3$-type structure the Si atoms occupy two different sites, and hence the stacking order of T and Si layers along the c axis is different in the two structures. The structural difference in the two structures is evident from Fig. 2. It is seen that the $BaNiSn_3$-type structure is not symmetric about the R plane and there is a loss of the mirror plane along the c axis in the $BaNiSn_3$-type structure which is present in the $ThCr_2Si_2$-type structure. The $ThCr_2Si_2$-type structure is centrosymmetric, whereas the $BaNiSn_3$-type structure is noncentrosymmetric.

IV. ELECTRICAL RESISTIVITY

The electrical resistivity ρ of $LaIrSi_3$ as a function of T for $0.35\ \text{K} \leqslant T \leqslant 300\ \text{K}$ measured at applied magnetic field $H = 0$ is shown in Fig. 3(a). A metallic behavior is inferred from the T dependence of ρ; ρ decreases with decreasing T, becomes nearly constant in the low-T limit below 25 K, and undergoes a sharp transition to a zero-resistance state due to the occurrence of superconductivity. It is seen that the onset of superconductivity takes place at $T_{c\,onset} \approx 1.6$ K, and the zero-resistivity state is reached at $T_{c\,0} \approx 1.3$ K. Thus a $T_c = 1.45$ K (defined as the midpoint of the transition) is obtained from the resistivity data. The $\rho(T)$ data at various H for $0 \leqslant H \leqslant$

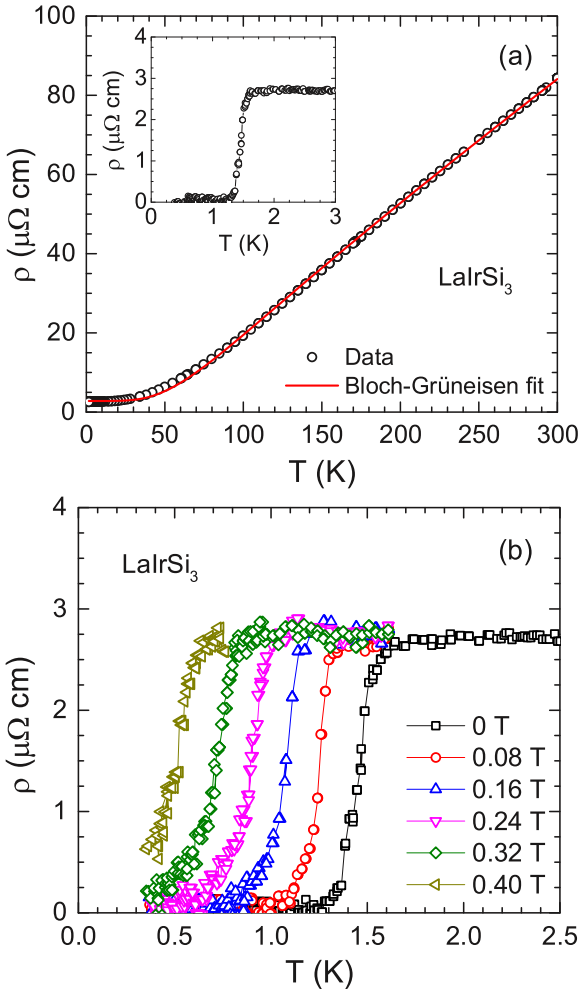

FIG. 3. (Color online) (a) Electrical resistivity ρ of $LaIrSi_3$ as a function of temperature T for 1.6 K $\leqslant T \leqslant$ 300 K measured in applied magnetic field $H = 0$. The red solid curve is a fit of $\rho(T)$ data by the Bloch-Grüneisen model. Inset: Expanded view of $\rho(T)$ below 3 K to show the superconductivity. (b) $\rho(T)$ of $LaIrSi_3$ for 0.35 K $\leqslant T \leqslant$ 2.5 K, showing the superconducting transitions for different values of H.

0.4 T are shown in Fig. 3(b). It is seen that T_c decreases with increasing H; at $H = 0.32$ T, T_c decreases to 0.70 K from 1.45 K at $H = 0$.

From Fig. 3(a) the residual resistivity before entering the superconducting state is $\rho_0 = 2.7\,\mu\Omega$ cm, and a residual resistivity ratio (RRR) $\equiv \rho(300\,\mathrm{K})/\rho(1.6\,\mathrm{K}) \approx 31$. The low value of ρ_0 and high value of RRR indicate good sample quality. In the normal state, the $\rho(T \geqslant 1.6\,\mathrm{K})$ data are well described by the Bloch-Grüneisen (BG) model of resistivity due to the scattering of conduction electrons by longitudinal acoustic lattice vibrations [45]. We fitted our normal-state $\rho(T)$ data by

$$\rho(T) = \rho_0 + \rho_{\mathrm{BG}}, \tag{1}$$

where

$$\rho_{\mathrm{BG}}(T/\Theta_{\mathrm{R}}) = 4\mathcal{R}\left(\frac{T}{\Theta_{\mathrm{R}}}\right)^5 \int_0^{\Theta_{\mathrm{R}}/T} \frac{x^5}{(e^x - 1)(1 - e^{-x})} dx \tag{2}$$

represents the BG resistivity. Θ_{R} is the Debye temperature from the resistivity data, and $\mathcal{R}$ is a material-dependent prefactor.

Our fit of $\rho(T)$ data in 1.6 K $\leqslant T \leqslant$ 300 K by the BG model is shown by the solid red curve in Fig. 3(a), where we used an analytic Padé approximant fitting function for ρ_{BG} from Ref. [46]. From the fitting of $\rho(T)$ data we obtain $\rho_0 = 2.81(2)\,\mu\Omega$ cm, $\Theta_{\mathrm{R}} = 331(2)$ K, and $\mathcal{R} = 95.7\,\mu\Omega$ cm. Further details about the fitting of $\rho(T)$ using the Bloch-Grüneisen model of resistivity can be found in Refs. [46,47].

V. HEAT CAPACITY

The heat capacity C_{p} of $LaIrSi_3$ as a function of T for 0.35 K $\leqslant T \leqslant$ 300 K measured at $H = 0$ is shown in Fig. 4(a). As shown in the inset, a sharp jump is observed in C_{p} due to the superconducting transition at $T_c = 0.72(1)$ K. The observation of such a sharp jump in $C_{\mathrm{p}}(T)$ indicates the occurrence of bulk superconductivity in $LaIrSi_3$. The $C_{\mathrm{p}}(T)$ data measured at different magnetic fields are shown in Fig. 4(b). It is seen that the jump ΔC_{p} in C_{p} and T_c decrease with the increasing H. T_c is found to decrease to 0.44(2) K at $H = 5.0$ mT from its value of $T_c = 0.72(1)$ K at $H = 0$, and it is suppressed to a temperature below 0.35 K by a field of $H = 7.0$ mT. The suppression of T_c with H for $C_{\mathrm{p}}(T,H)$ is very different from that observed for the $\rho(T,H)$ data above, where superconductivity survives even at an applied field of 0.4 T.

The low-temperature normal-state heat-capacity data are well described by $C_{\mathrm{p}}(T) = \gamma_{\mathrm{n}}T + \beta T^3$. The normal-state Sommerfeld electronic heat-capacity coefficient γ_{n} is estimated by fitting the normal-state $C_{\mathrm{p}}(T)$ data measured at $H = 0$ (at 0.75 K $\leqslant T \leqslant$ 3.8 K) and at $H = 10.0$ mT (at 0.35 K $\leqslant T \leqslant$ 0.9 K) simultaneously. The simultaneous linear fit of $C_{\mathrm{p}}(T)/T$ versus T^2 by $C_{\mathrm{p}}(T)/T = \gamma_{\mathrm{n}} + \beta T^2$ at 0.35 K $\leqslant T \leqslant$ 3.8 K yields $\gamma_{\mathrm{n}} = 4.60(2)$ mJ/mol K^2 and $\beta = 0.17(1)$ mJ/mol K^4. The coefficient β according to the relation [48] $\Theta_{\mathrm{D}} = (12\pi^4 Rp/5\beta)^{1/3}$, where R is the molar gas constant and $p = 5$ is the number of atoms per formula unit, gives the Debye temperature $\Theta_{\mathrm{D}} = 385(8)$ K. The experimental $C_{\mathrm{p}}(T = 300\mathrm{K}) \approx 106$ J/mol K does not reach the Dulong-Petit high-T limit of the lattice heat capacity $C_V = 3pR = 15R = 124.7$ J/mol K.

The coefficient γ_{n} can be used to estimate the density of states at the Fermi level $\mathcal{D}(E_{\mathrm{F}})$, which, according to the relation [48] $\gamma_{\mathrm{n}} = (\pi^2 k_{\mathrm{B}}^2/3)\,\mathcal{D}(E_{\mathrm{F}})$, gives $\mathcal{D}(E_{\mathrm{F}}) = 1.95(1)$ states/eV f.u. for both spin directions. This $\mathcal{D}(E_{\mathrm{F}})$ contains the quasiparticle mass enhancement by many-body electron-phonon interaction and is related to the bare density of states $\mathcal{D}_{\mathrm{band}}(E_{\mathrm{F}})$ by [49] $\mathcal{D}(E_{\mathrm{F}}) = (1 + \lambda_{\mathrm{e-ph}})\mathcal{D}_{\mathrm{band}}(E_{\mathrm{F}})$, where $\lambda_{\mathrm{e-ph}}$ is the electron-phonon coupling constant that can be estimated from Θ_{D} and T_c using McMillan's relation [50],

$$\lambda_{\mathrm{e-ph}} = \frac{1.04 + \mu^* \ln(\Theta_{\mathrm{D}}/1.45\,T_c)}{(1 - 0.62\mu^*)\ln(\Theta_{\mathrm{D}}/1.45\,T_c) - 1.04}. \tag{3}$$

Here μ^* is the repulsive screened Coulomb parameter usually assigned as $\mu^* = 0.13$. For $LaIrSi_3$ we have $T_c = 0.72$ K and $\Theta_{\mathrm{D}} = 385$ K, which together with $\mu^* = 0.13$, according to Eq. (3), give $\lambda_{\mathrm{e-ph}} = 0.41$. The small value of $\lambda_{\mathrm{e-ph}}$ implies a weak-coupling superconductivity in $LaIrSi_3$. This value of $\lambda_{\mathrm{e-ph}}$ combined with $\mathcal{D}(E_{\mathrm{F}}) = 1.95(1)$ states/eV f.u. for both

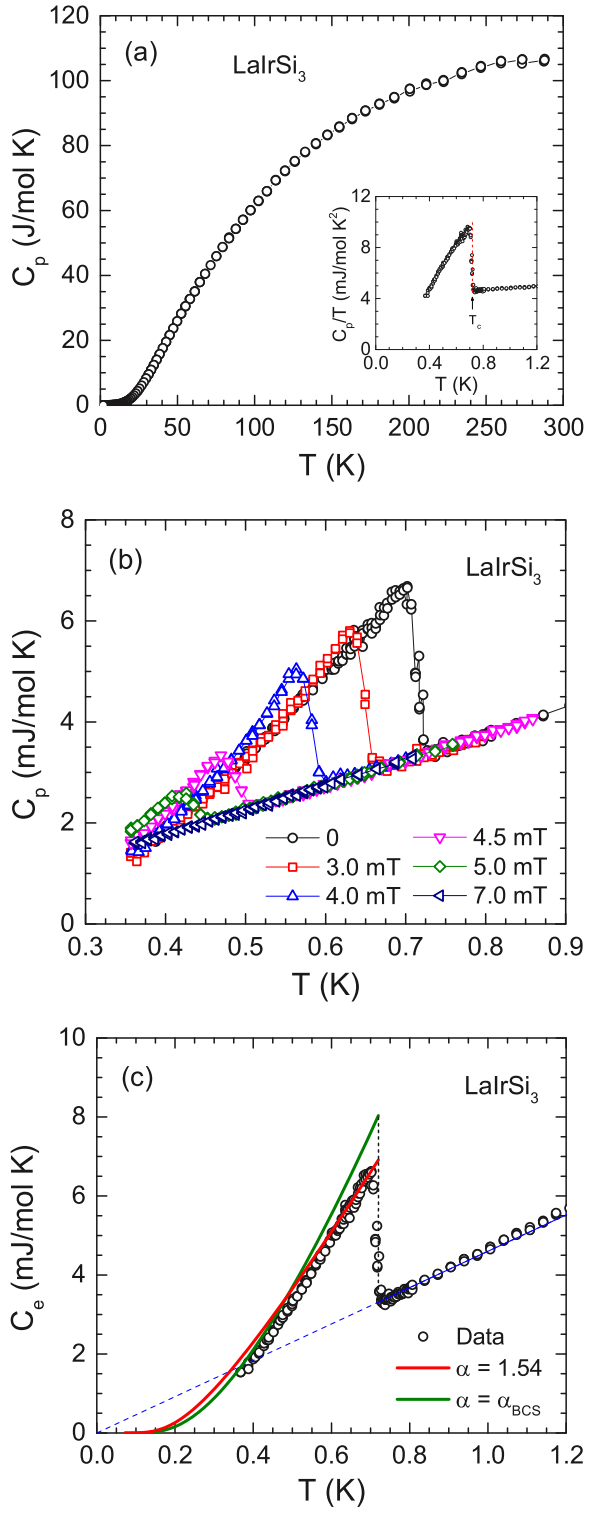

FIG. 4. (Color online) (a) Heat capacity C_p of $LaIrSi_3$ as a function of temperature T for 1.8 K $\leqslant T \leqslant$ 300 K measured in zero magnetic field. Inset: C_p/T vs T for 0.35 K $\leqslant T \leqslant$ 1.2 K. The dotted red line marks the superconducting transition temperature T_c. (b) $C_p(T)$ for 0.35 K $\leqslant T \leqslant$ 0.9 K measured in different applied magnetic fields. (c) Electronic contribution C_e to zero-field heat capacity as a function of temperature T. The solid red curve is the theoretical prediction of the α model for $\alpha = \Delta(0)/k_B T_c = 1.54$. The BCS prediction for $\alpha_{BCS} = 1.764$ is also shown for comparison.

spin directions gives $\mathcal{D}_{band}(E_F) = 1.38(1)$ states/eV f.u. for both spin directions. The effective mass m^* of the quasiparticle can be obtained from $m^* = (1 + \lambda_{e-ph})\, m^*_{band}$, which gives $m^* = 1.41\, m_e$, assuming the effective band mass $m^*_{band} = m_e$, the free electron mass.

The density of states and hence γ_n can be further used to estimate the Fermi velocity v_F, which is related to $\mathcal{D}(E_F)$ by [48] $v_F = (\pi^2\hbar^3/m^{*2}V_{f.u.})\mathcal{D}(E_F)$, where $\hbar$ is Planck's constant divided by 2π and $V_{f.u.} = V_{cell}/2$ is the volume per formula unit. We thus estimate $v_F = 9.49 \times 10^7$cm/s for $LaIrSi_3$ using the above-estimated $\mathcal{D}(E_F)$ and m^*. v_F together with ρ_0 can be used to estimate the mean free path ℓ, as $\ell = v_F\tau$, and the mean free scattering time $\tau = m^*/ne^2\rho_0$, with the conduction carrier density $n = m^{*3}v_F^3/3\pi^2\hbar^3$, assuming a spherical Fermi surface [48]. Combining all these,

$$\ell = 3\pi^2\left(\frac{\hbar}{e^2\rho_0}\right)\left(\frac{\hbar}{m^* v_F}\right)^2, \tag{4}$$

which for $\rho_0 = 2.7\ \mu\Omega$ cm and the above-estimated v_F and m^* gives $\ell = 33.7$ nm.

VI. SUPERCONDUCTING-STATE PROPERTIES

The electronic contribution to the heat capacity $C_e(T)$ after subtracting the phonon contribution from the measured $C_p(T)$ data, i.e., $C_e(T) = C_p(T) - \beta T^3$, is shown in Fig. 4(c), which clearly shows the sharp jump in C_e at T_c. The jump ΔC_e in C_e at T_c is found to be $\Delta C_e = 3.6(1)$ mJ/mol K, corresponding to the vertical dotted line at T_c in Fig. 4(c). This gives $\Delta C_e/\gamma_n T_c = 1.09(3)$ for $\gamma_n = 4.60(2)$ mJ/mol K^2 and $T_c = 0.72(1)$ K, which is significantly smaller than the BCS value of $\Delta C_e/\gamma_n T_c = 1.43$ in the weak-coupling limit [51]. The presence of a residual heat capacity due to a small impurity/nonsuperconducting phase can lead to a reduced $\Delta C_e/\gamma_n T_c$. However, in view of the fact that the jump in $C_e(T)$ at the superconducting transition is very sharp, the entire sample seems to be superconducting without any residual γ, which in turn suggests that the reduction in $\Delta C_e/\gamma_n T_c$ is intrinsic. In a single-band model, such a reduction can be caused by the presence of an anisotropic superconducting energy gap (order parameter) in momentum space [38]. That the reduction in $\Delta C_e/\gamma_n T_c$ is intrinsic will be clear from our analysis of the superconducting-state data using the single-band α model of BCS superconductivity [38–40] below, which is applicable to the system with $\Delta C_e/\gamma_n T_c \neq 1.43$.

In the so-called α model of BCS superconductivity in order to fit the superconducting-state thermodynamic data, $\alpha_{BCS} \equiv \Delta(0)/k_B T_c = 1.764$ is replaced by a variable α [38,39]. α is determined from the jump ΔC_e at T_c according to the relation [38]

$$\frac{\Delta C_e(T_c)}{\gamma_n T_c} = 1.426\left(\frac{\alpha}{\alpha_{BCS}}\right)^2, \tag{5}$$

which for $\Delta C_e/\gamma_n T_c = 1.09(3)$ gives $\alpha = 1.54(2)$. This value of α is significantly smaller than the BCS value of 1.764. The temperature dependence of α-model superconducting-state heat capacity $C_e(T)$ calculated for $\alpha = 1.54$ is shown by the solid red curve in Fig. 4(c) together with that of the BCS prediction for $\alpha = \alpha_{BCS}$. A reasonable agreement is observed

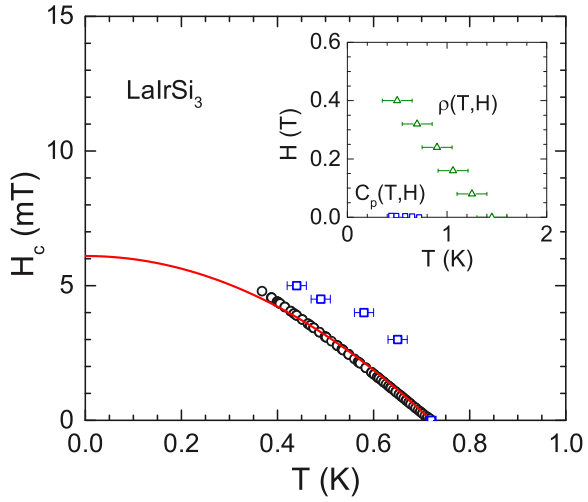

FIG. 5. (Color online) Thermodynamic critical field H_c of $LaIrSi_3$ as a function of temperature T obtained from the experimental electronic heat capacity $C_e(T)$ data. The H-dependent T_c obtained from the heat capacity $C_p(T,H)$ data in Fig. 4(b) are also shown by open squares. The solid line represents the parabolic fit to $H_c(T) = H_c(0)[1-(T/T_c)^2]$, as discussed in the text. Inset: H-T phase diagram obtained from the electrical resistivity $\rho(T,H)$ in Fig. 3(b) together with $T_c(H)$ from $C_p(T,H)$.

between the α-model prediction and the superconducting-state $C_e(T)$ data, which supports the applicability of the α model and in turn indicates that the s-wave order parameter of $LaIrSi_3$ is anisotropic in momentum space. The details about the fitting of $C_e(T)$ data by the α model of BCS superconductivity can be found in Refs. [38,52]. The lack of perfect agreement between the α-model prediction and the experimental data may indicate that the anisotropy of the gap is not well accounted for, as the simplified α model does not account for the energy dependence of the gap function or for a complex Δ.

The thermodynamic critical field H_c is estimated from the zero-field $C_e(T)$ data by integrating the entropy difference between the superconducting and normal states [51,53], $H_c^2(T) = 8\pi \int_T^{T_c}[S_{en}(T') - S_{es}(T')]dT'$, where S_{en} and S_{es} are the electronic entropy of normal and superconducting states, respectively, with $S_e(T') = \int_0^{T'}[C_e(T'')/T'')]dT''$. $H_c(T)$ obtained this way from the zero-field $C_e(T)$ is shown in Fig. 5. The T dependence of H_c can be approximated to the conventional relation $H_c(T) = H_c(0)[1-(T/T_c)^2]$, which gives $H_c(0) = 6.10(3)$ mT. The solid red curve in Fig. 5 represents the fit of $H_c(T)$ data with this expression.

The experimental $H_c(0)$ so obtained is somewhat higher than the theoretical $H_c(0)$, which for the α model is given by [38]

$$\frac{H_c(0)}{\left(\gamma_{nV}T_c^2\right)^{1/2}} = \sqrt{\frac{6}{\pi}}\,\alpha \approx 1.382\,\alpha, \tag{6}$$

where the Sommerfeld coefficient per unit volume γ_{nV} is in units of erg/cm^3 K^2. From this relation for $\alpha = 1.54$ we obtain $H_c(0) = 4.5$ mT, which is a little lower than $H_c(0) = 6.10(3)$ mT obtained above. Even for $\alpha_{BCS} = 1.764$, Eq. (6) gives a lower $H_c(0) = 5.1$ mT. The reason for this discrepancy between the experimental and theoretical values of $H_c(0)$ is not clear. We suspect that this might be the result of a nonspherical/anisotropic Fermi surface in $LaIrSi_3$ which is not properly accounted by equation (6).

Further, as can be seen from Fig. 5, $H_c(T)$ obtained from the zero-field $C_e(T)$ data and the H-T phase diagram determined from the H-dependent T_c from $C_p(T,H)$ data in Fig. 4(b) both give very low critical fields. For a type-II superconductivity $T_c(H)$ obtained from $C_p(T,H)$ gives the upper critical field H_{c2}, which is usually much higher than the thermodynamic critical field, which is not the present case. The fact that $H_{c2}(T)$ is close to $H_c(T)$ may suggest a type-I superconductivity in $LaIrSi_3$ or a type-1.5 behavior that may arise from the presence of split spin-up and spin-down energy bands similar to what has been observed in two-band superconductor MgB_2 [54].

The H-dependent T_c from $\rho(T,H)$ data in Fig. 3(b) is shown in the inset of Fig. 5, which shows a very different behavior than $T_c(H)$ from $C_p(T,H)$ data. This is consistent with the observation of different T_c in resistivity and heat-capacity measurements in zero field mentioned above, apparently due to the filamentary/surface superconductivity that sets in at a temperature higher than the bulk superconductivity. Our estimate of the Ginzburg-Landau parameter κ below gives $\kappa = 0.55$, which suggests a type-I behavior. Usually, for a type-I superconductor we do not expect a filamentary or surface superconductivity. However, surface superconductivity is predicted for a type-I superconductor with κ values between $1/\sqrt{2}$ and $1/2.39$ [55,56]. Indeed, our estimated κ lies between these limits, and we can expect a surface superconductivity in $LaIrSi_3$. The critical field associated with the surface superconductivity is given by [55,56] $H_{c3} = 2.39\,\kappa\,H_c$; accordingly, for $LaIrSi_3$ we estimate $H_{c3} = 8.0$ mT, which is much smaller than the observed upper critical field from the resistivity measurement (inset of Fig. 5). Thus the observed $T_c(H)$ from $\rho(T,H)$ could not be understood to arise from surface superconductivity. The reason for such a high critical field in the resistivity measurement of $LaIrSi_3$ is not clear. The type-I superconductor $LaPdSi_3$ was also found to exhibit a higher critical field in the resistivity measurement compared to that in the heat capacity [31]. In a recent study Kimura *et al.* [57] found a similar high critical field from the resistivity measurement on the type-I superconductor $LaRhSi_3$, and they argue that this behavior may be a common feature in noncentrosymmetric superconductors. However, we are not aware of any theoretical discussion of this aspect of noncentrosymmetric superconductors, and this hypothesis needs to be tested theoretically.

Our estimate of the superconducting London penetration depth in the clean limit at $T = 0$, $\lambda_L(0)$ from v_F using the relation [51]

$$\lambda_L(0)^2 = \frac{m^*c^2}{4\pi ne^2} = \frac{3\pi c^2\hbar^3}{4m^{*2}e^2v_F^3}, \tag{7}$$

where c is the speed of light in vacuum, gives $\lambda_L(0) = 25.9$ nm for $v_F = 9.49 \times 10^7$ cm/s. The BCS coherence length ξ_0 can be obtained from v_F and the energy gap $\Delta(0)$, which for the α model is given by [38]

$$\xi_0 = \frac{\hbar v_F}{\pi\,\Delta(0)} = \left(\frac{1}{\pi\alpha}\right)\frac{\hbar v_F}{k_B T_c}. \tag{8}$$

TABLE II. Measured and derived superconducting and relevant normal-state parameters for the noncentrosymmetric superconductor $LaIrSi_3$.

Parameter	Value
T_c (K)	0.72(1)
γ_n (mJ/mol K^2)	4.60(2)
Θ_D (K)	385(8)
λ_{e-ph}	0.41
ΔC_e (mJ/mol K)	3.6(1)
$\Delta C_e/\gamma_n T_c$	1.09(3)
$\alpha \equiv \Delta(0)/k_B T_c$ (from $\Delta C_e/\gamma_n T_c$)	1.54(2)
$\Delta(0)/k_B$ (K)	1.11
$H_c(T=0)$ (mT)	6.10(3)
κ_{GL}	0.55
$\xi(0)$ (nm)	373
ξ_0 (nm)	2081
ℓ (nm)	33.7
$\lambda_L(0)$ (clean limit) (nm)	25.9
$\lambda_{eff}(0)$ (dirty limit) (nm)	205

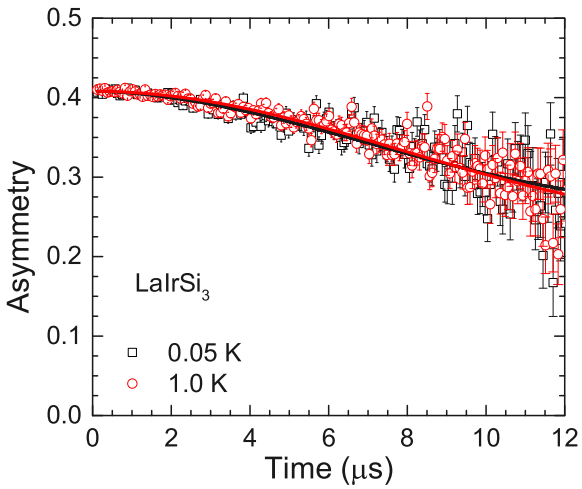

FIG. 6. (Color online) Zero-field μSR spectra of $LaIrSi_3$ measured in longitudinal geometry at temperatures above (1.0 K) and below (0.05 K) the superconducting T_c. The solid curves are the fits by the Gaussian Kubo-Toyabe function in Eq. (10).

This gives $\xi_0 = 2081$ nm for $\alpha = 1.54$ and $v_F = 9.49 \times 10^7$cm/s. We see that ξ_0 is much larger than the above-estimated mean free path $\ell = 33.7$ nm, $\ell/\xi_0 \approx 0.016 \ll 1$, suggesting that the superconductivity in $LaIrSi_3$ is in the dirty limit. In the dirty limit, the Ginzburg-Landau parameter $\kappa_{GL} = 0.715\,\lambda_L(0)/\ell$ [51], which gives $\kappa_{GL} = 0.55 < 1/\sqrt{2}$, as expected for a type-I superconductivity. This value of κ_{GL} is close to the value obtained using the dirty-limit relation for a fully gapped (isotropic) superconductor [58], $\kappa_{GL} = 7.49 \times 10^3 \rho_0 \sqrt{\gamma_n v}$, with ρ_0 in Ω cm, which gives $\kappa_{GL} = 0.59$. Both estimates of κ_{GL} consistently indicate a type-I superconductivity in $LaIrSi_3$.

The effective magnetic penetration depth λ_{eff} can be estimated using the relation [51]

$$\lambda_{eff}(0) = \lambda_L(0)\sqrt{1 + \frac{\xi_0}{\ell}} \qquad \text{(dirty limit)}, \tag{9}$$

which gives $\lambda_{eff}(0) = 205$ nm. Then, using the relation $\kappa_{GL} = \lambda_{eff}(0)/\xi(0)$, we estimate the Ginzburg-Landau coherence length $\xi(0)$, which for $\kappa_{GL} = 0.55$ yields $\xi(0) = 373$ nm. The measured and derived superconducting parameters of $LaIrSi_3$ are listed in Table II.

VII. MUON SPIN RELAXATION AND ROTATION

The time evolution of muon spin relaxation in zero field (ZF) is shown in Fig. 6 for T both above and below the bulk T_c. It is evident from the ZF μSR spectra that there is no noticeable change in the relaxation rates at 1.0 K ($>T_c$) and 0.05 K ($<T_c$). This indicates that the time-reversal symmetry remains preserved upon entering the superconducting state. The ZF μSR spectra are best described by the Gaussian Kubo-Toyabe function,

$$G_z(t) = A_0\left[\tfrac{1}{3} + \tfrac{2}{3}(1-\sigma^2 t^2)e^{-\sigma^2 t^2/2}\right]e^{-\lambda t} + A_{BG}, \tag{10}$$

where A_0 is the initial asymmetry, σ and λ are the depolarization rates, and A_{BG} is the time-independent background contribution. σ accounts for the Gaussian distribution of static fields from nuclear moments (the local field distribution width $\langle H_\mu \rangle = \sigma/\gamma_\mu$, with muon gyromagnetic ratio $\gamma_\mu = 135.53$ MHz/T), and λ accounts for the electronic moments. The fits of μSR spectra in Fig. 6 by the decay function in Eq. (10) give $\sigma = 0.074(1)$ μs^{-1} and $\lambda = 0.009(3)$ μs^{-1} at 1.0 K and $\sigma = 0.074(1)$ μs^{-1} and $\lambda = 0.011(2)$ μs^{-1} at 0.05 K. The fits are shown by the solid red curve in Fig. 6. Since within the error bars both σ and λ at $T < T_c$ and $T > T_c$ are similar, there is no evidence of time-reversal symmetry breaking in $LaIrSi_3$.

The time evolution of muon spin rotation in transverse field (TF) is shown in Fig. 7. The TF muon spin precession signals were collected on a field-cooled sample at different applied fields both above (1.0 K) and below (0.05 K) T_c. The TF μSR spectra are best described by an oscillatory function damped with a Gaussian and an oscillatory background, i.e., by

$$G_z(t) = A_0 \cos(\omega t + \varphi)e^{-\sigma^2 t^2/2} + A_{BG}\cos(\omega t + \varphi), \tag{11}$$

where $\omega = \gamma_\mu H_{int}$ is the precession frequency (H_{int} is the internal field at the muon site). Solid curves in Fig. 7 are the fits of the TF μSR spectra by the decay function in Eq. (11). In the superconducting state at $T = 0.05$ K the depolarization rate is found to increase significantly; for example, for the TF μSR spectra at 2.5 mT, σ increases from its value $\sigma = 0.010(2)$ μs^{-1} at 1.0 K to $\sigma = 1.45(4)$ μs^{-1} at 0.05 K. Such an increase of the depolarization rate reveals bulk superconductivity in $LaIrSi_3$.

The maximum entropy spectra for TF μSR precession at 1.0 and 0.05 K are shown in Fig. 8. The maximum entropy spectra depict the magnetic field probability distribution $P(H)$. It is clear from Fig. 8 that at 1.0 K (in the normal state) sharp peaks are observed at H_{int} exactly equal to the applied H, whereas at 0.05 K (in the superconducting state) one can see additional peaks. At $H = 4.0$ mT, $P(H)$ at 0.05 K shows an additional peak at $H_{int} > H$ (inset of Fig. 8). The appearance of an additional peak (near 5.5 mT, which gives an estimation of H_c) at an internal field greater than the applied H is a characteristic

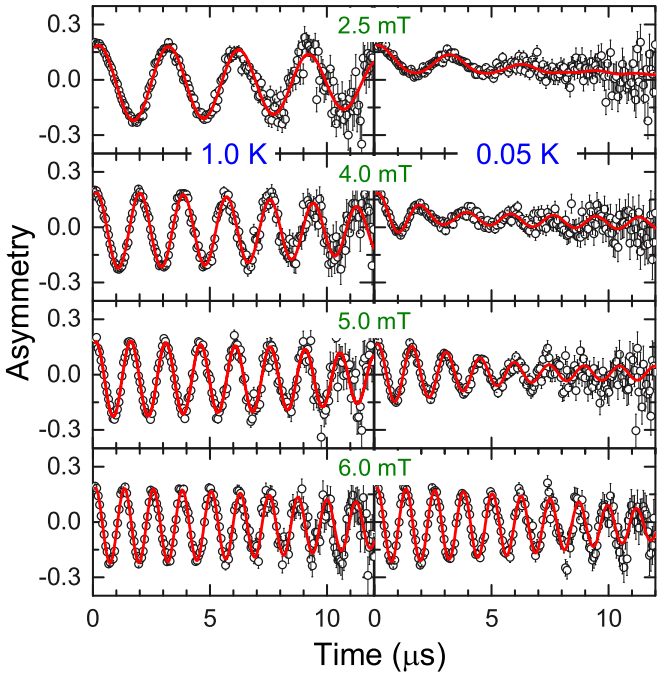

FIG. 7. (Color online) The transverse field μSR spectra at temperatures above (1.0 K, left panels) and below (0.05 K, right panels) the superconducting T_c for the indicated applied fields. The solid curves are the fits by the oscillatory function in Eq. (11).

of a type-I behavior and indicates a type-I superconductivity in $LaIrSi_3$ consistent with the above inference from the value of κ_{GL} in Table II. Further at 0.05 K for $H \leqslant 4.0$ mT we also observe an increase in $P(H)$ near $H_{int} \sim 0.5$ mT, as is expected for a sample in the Meissner state. However, no such

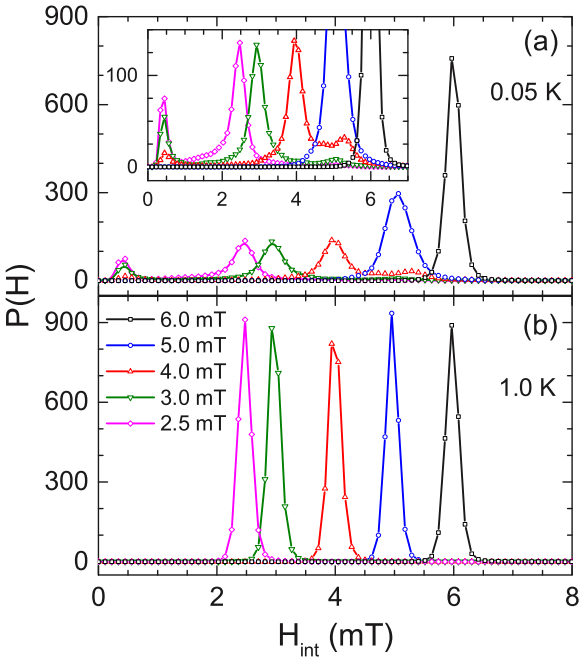

FIG. 8. (Color online) The maximum entropy spectra at different applied fields H for (a) 0.05 K and (b) 1.0 K. The inset in (a) shows an expanded view of the magnetic field probability distribution $P(H)$.

increase in $P(H)$ is observed from the Meissner volume in the intermediate state (i.e., at $H = 5.0$ mT). At $H = 6.0$ mT no additional peak is observed in $P(H)$ at $H_{int} > H$ even on an expanded scale. This could be understood to be due to the fact that the applied H is close to $H_c = 6.1$ mT (see Table II) and the sample is on the verge of a transition from a superconducting to a normal state at $H = 6.0$ mT. Thus the μSR data also reflect a low thermodynamic critical field $H_c \approx 5.5$ mT, in line with the estimate of H_c from the heat-capacity data.

VIII. CONCLUSIONS

The superconducting and normal-state properties of the noncentrosymmetric superconductor $LaIrSi_3$, which crystallizes in a $BaNiSn_3$-type tetragonal crystal structure (space group $I4mm$), were investigated using $C_p(T,H)$, $\rho(T,H)$, and μSR measurements which demonstrate bulk BCS superconductivity below $T_c = 0.72(1)$ K. A nonbulk superconductivity sets in at a higher T_c in $\rho(T)$. In the normal state ρ exhibits metallic behavior, and $\rho(T \geqslant 1.6\,\text{K})$ is well described by the Bloch-Grüneisen model of resistivity. Our analysis of low-temperature normal-state $C_p(T)$ data yields a Sommerfeld coefficient $\gamma_n = 4.60(2)\,\text{mJ/mol K}^2$, corresponding to the density of states at Fermi energy $\mathcal{D}(E_F) = 1.95(1)$ states/eV f.u. for both spin directions.

The superconducting transition is revealed by a very sharp jump in C_p at $T_c = 0.72(1)$ K, however, with a value of $\Delta C_e/\gamma_n T_c = 1.09(3)$ lower than the BCS expected value of 1.43. The reduced value of $\Delta C_e/\gamma_n T_c$ seems to indicate an anisotropic energy gap in $LaIrSi_3$. The superconducting-state electronic heat-capacity data are analyzed by the single-band α model of BCS superconductivity that describes the experimental data reasonably. $\alpha = \Delta(0)/k_B T_c = 1.54(2)$ obtained from the jump in C_p is smaller than $\alpha_{BCS} = 1.764$, indicating the s-wave order parameter of $LaIrSi_3$ is anisotropic in momentum space. Even though the single-band α model describes the superconducting-state data reasonably, considering the split spin-up and spin-down bands in $LaIrSi_3$, the possibility of two-band superconductivity cannot be ruled out. The presence of two bands is also known to result in a reduced $\Delta C_e/\gamma_n T_c$ [38,59]. Since the two-band effect and an anisotropy modification to a single band have similar manifestations, it is very difficult to distinguish between them by examining the thermodynamic quantities. Recently, a two-band superconductivity with equal energy gaps was reported in $SrPt_3P$ [60]. Further investigations are desired to check for the possibility of a similar two-band single-gap superconductivity in $LaIrSi_3$.

Various normal- and superconducting-state parameters have been estimated which indicate a dirty-limit weak-coupling type-I s-wave BCS superconductivity in $LaIrSi_3$. Type-I superconductivity is further confirmed by μSR. The μSR measurement also revealed that the time-reversal symmetry is preserved in the superconducting state, thus confirming a conventional s-wave singlet pairing superconductivity in $LaIrSi_3$. Thus, despite a large splitting of Fermi surfaces due to antisymmetric coupling on account of the noncentrosymmetric structure inferred from the de Haas–van Alphen effect study [33], no clear signature of parity mixing or a

spin-triplet pairing state is found in our investigations of the superconducting-state properties of $LaIrSi_3$.

The type-I superconductivity in $LaIrSi_3$ is similar to that of NCS $LaRhSi_3$, which also exhibits conventional s-wave electron-phonon-mediated type-I superconductivity with preserved time-reversal symmetry and a singlet pairing [26]. $LaRhSi_3$ and $LaIrSi_3$ have similar $\mathcal{D}(E_F)$ and Θ_D; therefore one would expect the T_c of these two compounds to be similar; however, we see that $T_c = 0.72(1)$ K for $LaIrSi_3$ is significantly lower than $T_c = 2.16(8)$ K for $LaRhSi_3$ [26]. While the reason for this contrasting behavior is not clear, T_c appears to have a relation with the outer-shell electronic configuration of Rh ($4d$) and Ir ($5d$) in these two superconductors. A similar trend has been observed in other $4d$ and $5d$ systems, such as in $LaPdSi_3$ [$T_c = 2.65(5)$ K] and $LaPtSi_3$ [$T_c = 1.52(6)$ K] [31] as well as in Li_2Pd_3B [$T_c = 6.7$ K] and Li_2Pt_3B [$T_c = 2.43$ K] [11]. The $4d$-based superconductors appear to have higher T_c than those with $5d$. Further investigations to understand this aspect of superconductivity in these compounds are desired.

The effect of the lack of inversion symmetry on the superconducting properties of $LaIrSi_3$ does not seem to be pronounced despite a large splitting of spin-up and spin-down energy bands due to ASOC. Similar behavior is reported for NCS $BaPtSi_3$ [21], for which electronic-structure calculations revealed the splitting of bands because of spin-orbit interactions; however, the superconductivity turned out to be conventional BCS-like with a singlet paring. Such observations raise an important question: what else besides ASOC controls the appearance of anomalous superconducting state in a noncentrosymmetric system? The anomalous superconducting properties of the Ce-based strongly correlated NCSs, such as $CePt_3Si$ [9], $CeRhSi_3$ [13], and $CeIrSi_3$ [14] can naively be related to the magnetic pairing due to the presence of $4f$ moments. However, the unusual superconducting properties of weakly correlated NCSs Li_2Pt_3B [11], $LaNiC_2$ [19,20], and Re_6Zr [30] are not then obvious as they do not show any evidence of magnetic order. An important difference between the two groups of nonmagnetic NCSs, i.e., those exhibiting unusual superconducting properties and those exhibiting conventional superconductivity, is the difference in their crystal structures/space groups. This may suggest that these two groups of nonmagnetic NCSs may have different Fermi surface topologies that may have some role in realizing the effect of ASOC. A comparative study of the extent of ASOC in nonmagnetic NCSs, preferably by a technique that can directly probe Fermi surface topology, such as angle-resolved photoemission spectroscopy, complemented with band-structure calculations can shed light on this issue and would be of help in understanding the relationship between ASOC, Fermi surface topology, and anomalous superconductivity in NCSs.

ACKNOWLEDGMENTS

V.K.A., D.T.A. and A.D.H. acknowledge financial assistance from CMPC-STFC Grant No. CMPC-09108. A.B. thanks UJ and STFC for PDF funding. A.M.S. thanks the SA-NRF (78832) and the URC of UJ for financial assistance.

[1] *Non-centrosymmetric Superconductors: Introduction and Overview*, edited by E. Bauer and M. Sigrist, Lecture Notes in Physics (Springer, Berlin, 2012), Vol. 847.
[2] V. M. Édel'shteĭn, Zh. Eksp. Teor. Fiz. **95**, 2151 (1989) [Sov. Phys. JETP **68**, 1244 (1989)].
[3] L. P. Gor'kov and E. I. Rashba, Phys. Rev. Lett. **87**, 037004 (2001).
[4] K. V. Samokhin, E. S. Zijlstra, and S. K. Bose, Phys. Rev. B **69**, 094514 (2004).
[5] P. A. Frigeri, D. F. Agterberg, A. Koga, and M. Sigrist, Phys. Rev. Lett. **92**, 097001 (2004).
[6] S. Fujimoto, J. Phys. Soc. Jpn. **76**, 051008 (2007).
[7] E. Bauer, G. Hilscher, H. Michor, C. Paul, E. W. Scheidt, A. Gribanov, Y. Seropegin, H. Noel, M. Sigrist, and P. Rogl, Phys. Rev. Lett. **92**, 027003 (2004).
[8] E. Bauer, I. Bonalde, and M. Sigrist, Low Temp. Phys. **31**, 748 (2005).
[9] E. Bauer, H. Kaldarar, A. Prokofiev, E. Royanian, A. Amato, J. Sereni, W. Bramer-Escamilla, and I. Bonalde, J. Phys. Soc. Jpn. **76**, 051009 (2007).
[10] K. Togano, P. Badica, Y. Nakamori, S. Orimo, H. Takeya, and K. Hirata, Phys. Rev. Lett. **93**, 247004 (2004).
[11] H. Q. Yuan, D. F. Agterberg, N. Hayashi, P. Badica, D. Vandervelde, K. Togano, M. Sigrist, and M. B. Salamon, Phys. Rev. Lett. **97**, 017006 (2006).
[12] N. Kimura, K. Ito, K. Saitoh, Y. Umeda, H. Aoki, and T. Terashima, Phys. Rev. Lett. **95**, 247004 (2005).
[13] N. Kimura, Y. Muro, and H. Aoki, J. Phys. Soc. Jpn. **76**, 051010 (2007).
[14] I. Sugitani, Y. Okuda, H. Shishido, T. Yamada, A. Thamizhavel, E. Yamamoto, T. D. Matsuda, Y. Haga, T. Takeuchi, R. Settai, and Y. Ōnuki, J. Phys. Soc. Jpn. **75**, 043703 (2006).
[15] R. Settai, I. Sugitani, Y. Okuda, A. Thamizhavel, M. Nakashima, Y. Ōnuki, and H. Harima, J. Magn. Magn. Mater. **310**, 844 (2007).
[16] G. Knebel, D. Aoki, G. Lapertot, B. Salce, J. Flouquet, T. Kawai, H. Muranaka, R. Settai, and Y. Ōnuki, J. Phys. Soc. Jpn. **78**, 074714 (2009).
[17] F. Honda, I. Bonalde, K. Shimizu, S. Yoshiuchi, Y. Hirose, T. Nakamura, R. Settai, and Y. Ōnuki, Phys. Rev. B **81**, 140507 (2010).
[18] V. K. Pecharsky, L. L. Miller, K. A. Gschneidner, Phys. Rev. B **58**, 497 (1998).
[19] A. D. Hillier, J. Quintanilla, and R. Cywinski, Phys. Rev. Lett. **102**, 117007 (2009).
[20] I. Bonalde, R. L. Ribeiro, K. J. Syu, H. H. Sung, and W. H. Lee, New J. Phys. **13**, 123022 (2011).
[21] E. Bauer, R. T. Khan, H. Michor, E. Royanian, A. Grytsiv, N. Melnychenko-Koblyuk, P. Rogl, D. Reith, R. Podloucky, E.-W. Scheidt, W. Wolf, and M. Marsman, Phys. Rev. B **80**, 064504 (2009).
[22] T. Shibayama, M. Nohara, H. A. Kotari, Y. Okamoto, Z. Hiroi, and H. Takagi, J. Phys. Soc. Jpn. **76**, 073708 (2007).
[23] K. Wakui, S. Akutagawa, N. Kase, K. Kawashima, T. Muranaka, Y. Iwahori, J. Abe, and J. Akimitsu, J. Phys. Soc. Jpn. **78**, 034710 (2009).
[24] T. Klimczuk, F. Ronning, V. Sidorov, R. J. Cava, and J. D. Thompson, Phys. Rev. Lett. **99**, 257004 (2007).

[25] A. B. Karki, Y. M. Xiong, I. Vekhter, D. Browne, P. W. Adams, D. P. Young, K. R. Thomas, J. Y. Chan, H. Kim, and R. Prozorov, Phys. Rev. B **82**, 064512 (2010).
[26] V. K. Anand, A. D. Hillier, D. T. Adroja, A. M. Strydom, H. Michor, K. A. McEwen, and B. D. Rainford, Phys. Rev. B **83**, 064522 (2011).
[27] G. Eguchi, D. C. Peets, M. Kriener, and Y. Maeno, E. Nishibori, Y. Kumazawa, K. Banno, S. Maki, and H. Sawa, Phys. Rev B **83**, 024512 (2011).
[28] P. K. Biswas, M. R. Lees, A. D. Hillier, R. I. Smith, W. G. Marshall, and D. McK. Paul, Phys. Rev. B **84**, 184529 (2011).
[29] A. B. Karki, Y. M. Xiong, N. Haldolaarachchige, S. Stadler, I. Vekhter, P. W. Adams, D. P. Young, W. A. Phelan, and J. Y. Chan, Phys. Rev. B **83**, 144525 (2011).
[30] R. P. Singh, A. D. Hillier, B. Mazidian, J. Quintanilla, J. F. Annett, D. McK. Paul, G. Balakrishnan, and M. R. Lees, Phys. Rev. Lett. **112**, 107002 (2014).
[31] M. Smidman, A. D. Hillier, D. T. Adroja, M. R. Lees, V. K. Anand, R. P. Singh, R. I. Smith, D. M. Paul, and G. Balakrishnan, Phys. Rev. B **89**, 094509 (2014).
[32] F. von Rohr, H. Luo, N. Ni, M. Wörle, and R. J. Cava, Phys. Rev. B **89**, 224504 (2014).
[33] Y. Okuda, Y. Miyauchi, Y. Ida, Y. Takeda, C. Tonohiro, Y. Oduchi, T. Yamada, N. D. Dung, T. D. Matsuda, Y. Haga, T. Takeuchi, M. Hagiwara, K. Kindo, H. Harima, K. Sugiyama, R. Settai, and Y. Ōnuki, J. Phys. Soc. Jpn. **76**, 044708 (2007).
[34] Y. Tada, N. Kawakami, and S. Fujimoto, Phys. Rev. B **81**, 104506 (2010).
[35] A. Thamizhavel, T. Takeuchi, T. D. Matsuda, Y. Haga, K. Sugiyama, R. Settai, and Y. Ōnuki, J. Phys. Soc. Jpn. **74**, 1858 (2005).
[36] P. Lejay, I. Higashi, B. Chevalier, J. Etourneau, and P. Hagenmuller, Mater. Res. Bull. **19**, 115 (1984).
[37] P. Haen, P. Lejay, B. Chevalier, B. Lloret, J. Etourneau, and M. Sera, J. Less Common Met. **110**, 321 (1985).
[38] D. C. Johnston, Supercond. Sci. Technol. **26**, 115011 (2013).
[39] H. Padamsee, J. E. Neighbor, and C. A. Shiffman, J. Low Temp. Phys. **12**, 387 (1973).
[40] J. Bardeen, L. N. Cooper, and J. R. Schrieffer, Phys. Rev. **108**, 1175 (1957).
[41] J. Rodríguez-Carvajal, Physica B **192**, 55 (1993); FULLPROF: LLB-JRC, Laboratoire Léon Brillouin, CEA-Saclay, Gif-sur-Yvette, France, 1996.
[42] A. C. Larson and R. B. Von Dreele, Los Alamos National Laboratory, Technical Report No. LAUR 86-748, 2004; B. H. Toby, J. Appl. Cryst. **34**, 210 (2001).
[43] N. Engel, H. F. Braun, and E. Parthé, J. Less Common Met. **95**, 309 (1983).
[44] E. Parthé, B. Chabot, H. F. Braun, and N. Engel, Acta Crystallogr. B **39**, 588 (1983).
[45] F. J. Blatt, *Physics of Electronic Conduction in Solids* (McGraw-Hill, New York, 1968).
[46] R. J. Goetsch, V. K. Anand, A. Pandey, and D. C. Johnston, Phys. Rev. B **85**, 054517 (2012).
[47] V. K. Anand, P. K. Perera, A. Pandey, R. J. Goetsch, A. Kreyssig, and D. C. Johnston, Phys. Rev B **85**, 214523 (2012).
[48] C. Kittel, *Introduction to Solid State Physics*, 8th ed. (Wiley, New York, 2005).
[49] G. Grimvall, Phys. Scr. **14**, 63 (1976).
[50] W. McMillan, Phys. Rev. **167**, 331 (1968).
[51] M. Tinkham, *Introduction to Superconductivity*, 2nd ed. (Dover, Mineola, NY, 1996).
[52] V. K. Anand, H. Kim, M. A. Tanatar, R. Prozorov, and D. C. Johnston, Phys. Rev. B **87**, 224510 (2013).
[53] P. G. de Gennes, *Superconductivity of Metals and Alloys* (Benjamin, New York, 1966).
[54] V. Moshchalkov, M. Menghini, T. Nishio, Q. H. Chen, A. V. Silhanek, V. H. Dao, L. F. Chibotaru, N. D. Zhigadlo, and J. Karpinski, Phys. Rev. Lett. **102**, 117001 (2009).
[55] D. Saint-James and P. G. de Gennes, Phys. Lett. **7**, 306 (1963).
[56] M. Strongin, A. Paskin, D. G. Schweitzer, O. F. Kammerer, and P. P. Craig, Phys. Rev. Lett. **12**, 442 (1964).
[57] N. Kimura, H. Ogi, K. Satoh, G. Ohsaki, K. Saitoh, H. Iida, and H. Aoki, JPS Conf. Proc. **3**, 015011 (2014).
[58] T. P. Orlando, E. J. McNiff, Jr., S. Foner, and M. R. Beasley, Phys. Rev. B **19**, 4545 (1979).
[59] M. Zehetmayer, Supercond. Sci. Technol. **26**, 043001 (2013).
[60] R. Khasanov, A. Amato, P. K. Biswas, H. Luetkens, N. D. Zhigadlo, and B. Batlogg, arXiv:1404.5473.